J. Korean Inst. Electr. Electron. Mater. Eng.
Vol. 38, No. 1, pp. 89-94 January 2025
doi: https://doi.org/10.4313/JKEM.2025.38.1.12
ISSN 1226-7945(Print), 2288-3258(Online)

Early Stage Report : Undergraduate Research

Synthesis of Monodisperse Iron Oxide Nanoparticles with Control of Surface Properties and Magnetization

Dongyeong Gim, Hyeokju Kwon, and Minjeong Ha
School of Materials Science and Engineering, Gwangju Institute of Science and Technology, Gwangju 61005, Korea

(Received November 4, 2024; Accepted November 6, 2024)

Abstract: Iron oxide nanoparticles (NPs) have gained significant attention for their broad applicability in biomedical imaging, soft robotics, and catalysis owing to their exceptional magnetic properties and biocompatibility. A key challenge in maximizing their functionality lies in achieving a uniform size distribution and dispersity, alongside strong interfacial affinity with the surrounding medium that are essential for optimizing magnetic behavior and processibility. In this study, we present a facile solvothermal synthesis of monodisperse iron oxide NPs with tunable size and controllable surface hydrophobicity by varying precursors, capping agents, and solvents. By varying these synthesis parameters, we demonstrate a clear correlation between NP size, dispersity, and key magnetic properties, including saturation magnetization (M_S) and coercivity (H_C). This advancement in synthesis methodology offers a reliable, efficient approach for producing high-quality iron oxide NPs, which makes possible for practical use of them across a range of technological and biomedical applications.

Keywords: Iron oxide nanoparticle, Solvothermal synthesis, Monodisperse, Magnetic, Hydrophobicity

Iron oxide nanoparticles (NPs) such as magnetite (Fe_3O_4) and maghemite (γ-Fe_2O_3) have gained significant attention due to their high saturation magnetization (M_S) [1], chemical stability [2], and low toxicity [3], expanding their range of applications such as biomedical imaging [4], soft robotics [5], environmental remediation [6], and catalysis [7]. The key consideration for the synthesis of iron oxide NPs is uniform size distribution since the magnetic properties of iron oxide NPs are strongly influenced by their size. For example, as the size of magnetic NPs decreases, the magnetic domain transitions from a multi-domain structure to a single domain, resulting in an increase in coercivity (H_C) [8]. However, below a certain critical diameter, the effects of thermal fluctuations become greater than the magnetic anisotropy energy, causing the H_C to decrease towards zero, which is called superparamagnetic behavior [9]. Additionally, as the NP size decreases, the increased surface area leads to a higher proportion of disordered magnetic moments on the surface, resulting in a reduction of M_S [10].

For the synthesis of uniform iron oxide NPs, various strategies have been proposed such as thermal decomposition [11,12], co-precipitation [13], sol-gel [14], and the solvothermal method [15,16]. Since the surface properties of iron oxide NPs need to be tailored according to their application, it is crucial to manage and adjust these properties effectively. Esmaeilnezhad et al. synthesized hydrophobic iron oxide via thermal decomposition using oleylamine as capping agent to create a recyclable catalyst aimed at improving oil combustion efficiency [7]. Tognato et al. synthesized hydrophilic polyethylene glycol-capped iron oxide NPs by co-precipitation and fabricated a biocompatible anisotropic hydrogel for cell guidance by mixing with methacryloyl gelatin hydrogel [17]. Park et al. fabricated hydrophilic iron oxide NPs by coating hydrophobic iron oxide

✉ **Minjeong Ha; minjeongha@gist.ac.kr**

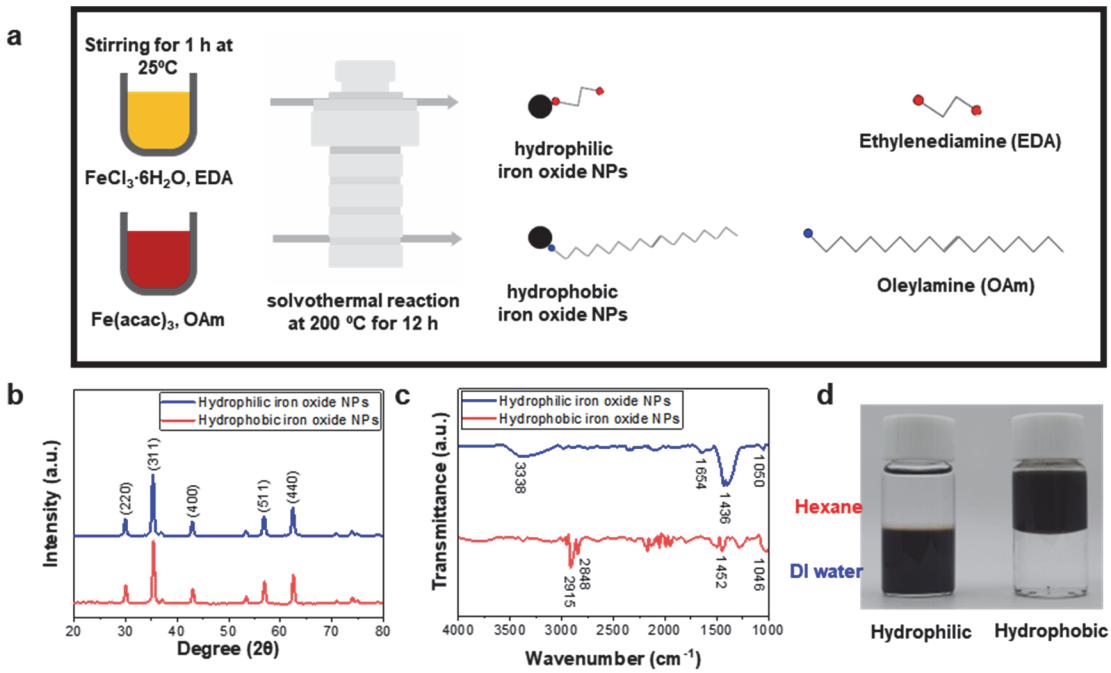

Fig. 1. (a) Schematic illustration of the synthesis of hydrophilic and hydrophobic iron oxide using the solvothermal method, (b) diffraction pattern of the synthesized iron oxide NPs, (c) FTIR analysis showing the surface properties of hydrophilic and hydrophobic iron oxide NPs, and (d) dispersion behavior of hydrophilic and hydrophobic iron oxide NPs.

NPs with dextran for use as a biomedical imaging contrast agent [4]. Consequently, various synthesis techniques or additional surface coatings have frequently been utilized to control surface properties for specific applications. However, altering synthesis methods or incorporating surface functionalization steps adds complexity to the process, increasing both time and costs. Among those, the solvothermal method has advantages such as facile control of size and phase by changing synthetic parameters [18]. Also, it is possible to control surface properties like hydrophilicity or hydrophobicity by changing the precursors, solvent, and capping agent without post-surface modification treatment.

In this study, a facile solvothermal synthesis of iron oxide NPs with monodispersity, size controllability, and optimized surface properties was proposed. To adjust the size of iron oxide NPs with specific surface properties, the concentration of the capping agent was varied, and the resulting morphologies and magnetic behaviors were studied. We obtained colloidal stability over 7 days in water and hexane for hydrophilic and hydrophobic iron oxide NPs, respectively. Additionally, the size of the NPs decreased to as small as 13.04 nm with increasing capping agent concentration. Finally, the strong correlation between the size of the NPs and magnetic properties was observed. As the particle size decreased, both hydrophilic and hydrophobic NPs approached superparamagnetic behavior, with M_S values ranging from 82 to 78 emu/g for hydrophilic NPs and 64 to 47 emu/g for hydrophobic NPs. This synthesis technique provides an efficient, reproducible method for producing high-quality iron oxide NPs, facilitating their practical applications across diverse technological and biomedical fields.

Figure 1(a) illustrates the synthetic procedures for hydrophilic and hydrophobic iron oxide NPs through the solvothermal method. For the synthesis of hydrophilic iron oxide NPs, 4 mmol of ferric chloride hexahydrate ($FeCl_3 \cdot 6H_2O$) was mixed with ethylenediamine (EDA) under vigorous magnetic stirring. Then 20 mL of ethylene glycol (EG) was added to the solution. In this process, EDA acts as a capping agent to stabilize Fe ions, regulating the growth rate of iron oxide NPs, while EG acts as a solvent and reducing agent to convert Fe^{2+} to Fe^{3+} [19,20]. The mixture was stirred vigorously for 1 h and then sealed in a 50 mL Teflon-lined stainless-steel autoclave. For synthesis of hydrophobic iron oxide NPs, 4 mmol of iron acetylacetonate [$Fe(acac)_3$] was

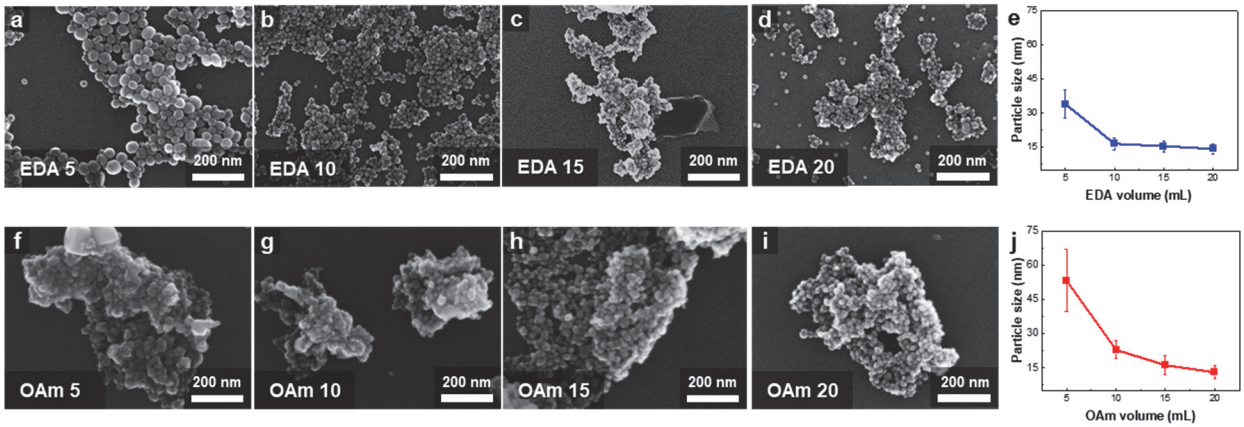

Fig. 2. (a-d) SEM images of hydrophilic iron oxide with different volume of EDA, (e) size variation with increasing volume of EDA, (f-i) SEM images of hydrophobic iron oxide with different volume of OAm, and (j) size variation with increasing volume of OAm.

mixed with hexane and oleylamine (OAm) under vigorous magnetic stirring for 1 h. In this case, OAm acts as both capping and reducing agent [21]. After mixing, the solution was poured into a 50 mL Teflon-lined stainless-steel autoclave. In both cases, the autoclave was maintained at 200℃ for 12 h with a heating rate of 2℃/min and then cooled to room temperature. The black solid product was obtained by rinsing with ethanol several times. Hydrophilic iron oxide NPs were re-dispersed in 2-propanol, and hydrophobic iron oxide NPs were re-dispersed in hexane for further analysis.

The crystal structure and surface composition were investigated using XRD and FTIR. In Fig. 1(b), the XRD peaks appeared at 30.1˚, 35.4˚, 42.3˚, 56.94˚, and 62.52˚, corresponding to the (220), (311), (400), (511), and (440) planes of Fe_3O_4, respectively, showing the high crystallinity of the iron oxide NPs [22]. Figure 1(c) illustrates the FTIR spectra of as-prepared iron oxide NPs. The broad band at 3,400~3,300 cm^{-1} in hydrophilic iron oxide NPs is caused by the stretching vibrations of OH and NH_2 groups. Peaks near 1,650 and 1,436 cm^{-1} exhibit NH_2 bending and CH_2 shear vibrations verifying the presence of EDA on the surface of the NPs. The C-N stretching vibrations are exhibited by peaks near 1,050 cm^{-1} [23]. Hydrophobic iron oxide NPs exhibit characteristic peaks of OAm since peaks near 2,850 and 2,920 cm^{-1} are caused by symmetric and asymmetric CH_2 stretching, and a weak peak near 1,500 cm^{-1} and 1,046 cm^{-1} is caused by C-C and C-N stretching of OAm [24]. From the FTIR analysis, the presence of the capping agent on the surface of the as-synthesized iron oxide NPs could be confirmed. These functional groups act as stabilizing agents for iron oxide NPs and determine hydrophobic or hydrophilic properties. To investigate the dispersion behavior of each type of NP based on their surface properties, hexane and water were used [Fig. 1(d)]. When the capping agent was EDA, the NPs dispersed only in water due to the presence of the polar NH_2 functional group. In contrast, when OAm was used as the capping agent, the NPs exhibited hydrophobicity by dispersing only in hexane due tp the long alkyl chain of OAm. Each type of NP maintained colloidal stability for over 7 days, remaining stably dispersed in the preferred solvent.

The synthesized iron oxide NPs varying capping agent volumes are shown in Fig. 2. The size of hydrophilic iron oxide NPs decreased from 34 nm to 14.3 nm as the size distribution became narrower with the increase in volume of EDA [Figs. 2(a)~(e)]. However, the morphology did not change significantly when the more than 10 mL of EDA was added. Similarly, the size of hydrophobic iron oxide NPs decreased from 53.27 nm to 13.04 nm with a narrower size distribution as the volume of OAm was increased [Figs. 2(f)~(j)]. Additionally, the effect of OAm was more significant than that of EDA, exhibiting a linear size reduction between 5~20 mL OAm volume. Since both EDA and OAm serve as capping agents, they are adsorbed on the nuclei produced in the early stage of synthesis. When the concentration of these capping agents is high, this adsorbed layer restricts the access of Fe ions to the nuclei, slowing down the crystal growth rate and yielding smaller NPs. Conversely, when the capping agent concentration is insufficient, the

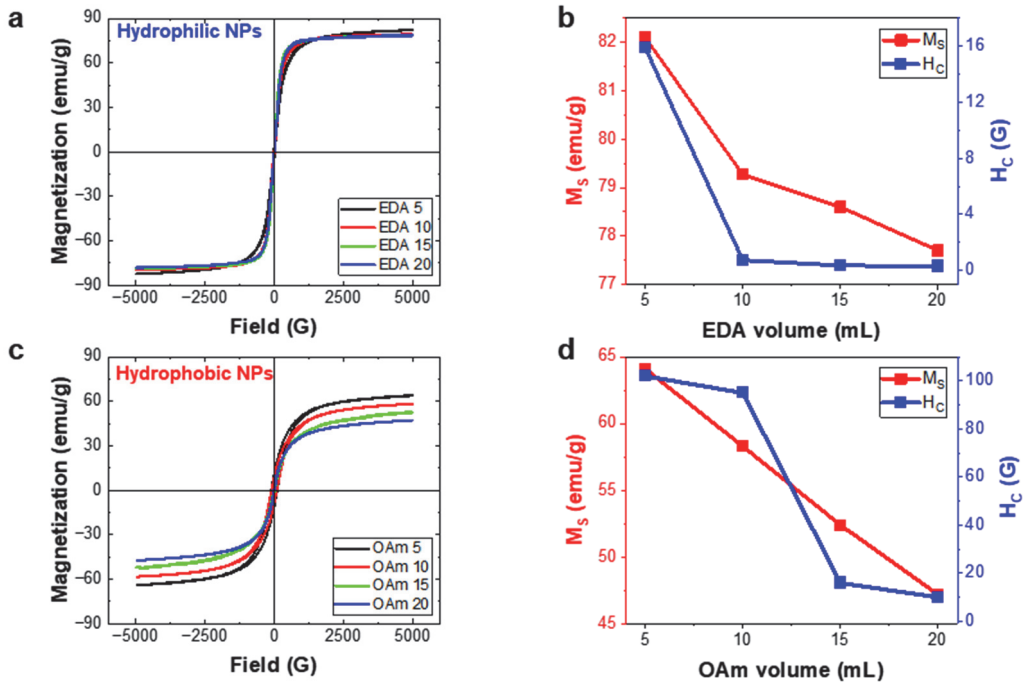

Fig. 3. (a) Magnetic properties of hydrophilic iron oxide NPs with increasing volume of EDA measured by VSM, (b) variation of M_S and H_C with varying volume of EDA, (c) magnetic properties of hydrophobic iron oxide NPs with increasing volume of OAm, and (d) variation of M_S and H_C with varying volume of OAm.

agents are only partially adsorbed on the nuclei, leading to irregular growth along the surface of the nuclei and non-uniform nanoparticles with larger diameters [19,21].

The magnetic properties of iron oxide NPs, which decreased in size as the volume of the capping agent increased, were investigated through VSM analysis (Fig. 3). For both hydrophilic and hydrophobic NPs, the increased volume of capping agent leads to decrease in size with lower saturation magnetization (M_S) and coercivity (H_C). In the case of M_S, hydrophilic NPs showed a small decrease in magnetization from 82 emu/g to 78 emu/g when the amount of EDA was increased from 5 ml to 20 ml [Figs. 3(a), (b)]. On the other hand, hydrophobic NPs exhibited a more significant decrease from 64 emu/g to 47 emu/g when the amount of OAm was increased from 5 ml to 20 ml [Figs. 3(c), (d)]. The larger reduction in M_S for the hydrophobic NPs compared to the hydrophilic NPs can be attributed to a more substantial decrease in particle size for the hydrophobic NPs. One important observation is that, at similar sizes, the hydrophilic NPs demonstrate a higher M_S. This can be linked to the reduction of Fe^{2+} ions to Fe^{3+} ions during the synthesis. For the hydrophilic NPs, EG serves as the reducing agent, whereas for the hydrophobic NPs, OAm takes on that role. Since EG is a stronger reducing agent compared to OAm, it facilitates a more efficient reduction of Fe^{3+} ions, leading to higher magnetization values for the hydrophilic NPs [25,26]. On the other hand, in terms of H_C, both samples exhibit a decrease to zero, indicating superparamagnetic behavior. This occurs when the particle size falls below the critical size for superparamagnetism in iron oxide, which is around 25 nm [9].

In conclusion, we successfully developed a facile solvothermal method to synthesize monodisperse iron oxide NPs with different surface properties by varying the precursors, solvent, and capping agent. Using EDA as a capping agent, we synthesized hydrophilic iron oxide NPs that can be dispersed in polar solvents due to the $-NH_2$ functional groups. When OAm was used as a capping agent, the long alkyl chains allowed the formation of hydrophobic NPs that disperse effectively in non-polar solvents. As the capping agents are adsorbed on the nuclei of NPs and restrict the access of Fe ion during the synthesis, we could produce smaller and more uniform iron oxide NPs by increasing the concentration

of capping agents. Additionally, as particle size decreased, we observed a reduction in M_S values and the emergence of superparamagnetic behavior, indicating a strong correlation between particle size and magnetic properties. Overall, this synthesis approach offers a simple and efficient route to produce iron oxide NPs with tailored sizes and surface properties, enhancing their potential for various applications in fields such as catalysis [7], biomedical imaging [4], and soft robotics [5].

ORCID

Minjeong Ha https://orcid.org/0000-0002-6635-7462

ACKNOWLEDGEMENT

This work was supported by the National Research Foundation of Korea (NRF) grant funded by the Korea government (MSIT) (No.RS-2023-00207836, 2022R1C1C10 04845).

REFERENCES

[1] Y. Hadadian, H. Masoomi, A. Dinari, C. Ryu, S. Hwang, S. Kim, B. K. Cho, J. Y. Lee, and J. Yoon, *ACS Omega*, **7**, 15996 (2022). doi: https://doi.org/10.1021/acsomega.2c01136

[2] E. Demangeat, M. Pédrot, A. Dia, M. Bouhnik-le-Coz, F. Grasset, K. Hanna, M. Kamagate, and F. Cabello-Hurtado, *Environ. Sci.: Nano*, **5**, 992 (2018). doi: https://doi.org/10.1039/C7EN01159H

[3] V. Valdiglesias, G. Kiliç, C. Costa, N. Fernández-Bertólez, E. Pásaro, J. P. Teixeira, and B. Laffon, *Environ. Mol. Mutagen.*, **56**, 125 (2015). doi: https://doi.org/10.1002/em.21909

[4] Y. I. Park, Y. Piao, N. Lee, B. Yoo, B. H. Kim, S. H. Choi, and T. Hyeon, *J. Mater. Chem.*, **21**, 11472 (2011). doi: https://doi.org/10.1039/C1JM10432B

[5] T. Jiralerspong, G. Bae, J. H. Lee, and S. K. Kim, *ACS Nano*, **14**, 17589 (2020). doi: https://doi.org/10.1021/acsnano.0c08346

[6] L. Mounier, M. Pédrot, M. Bouhnik-Le-Coz, and F. Cabello-Hurtado, *Environ. Sci.: Adv.*, **2**, 767 (2023). doi: https://doi.org/10.1039/D2VA00283C

[7] E. Esmaeilnezhad, M. Karimian, and H. J. Choi, *J. Ind. Eng. Chem.*, **71**, 402 (2019). doi: https://doi.org/10.1016/j.jiec.2018.11.052

[8] H. Kwon, Y. Yang, G. Kim, D. Gim, and M. Ha, *Nanoscale*, **16**, 6778 (2024). doi: https://doi.org/10.1039/D3NR05737B

[9] C. T. Yavuz, J. T. Mayo, W. W. Yu, A. Prakash, J. C. Falkner, S. Yean, L. Cong, H. J. Shipley, A. Kan, M. Tomson, D. Natelson, and V. L. Colvin, *Science*, **314**, 964 (2006). doi: https://doi.org/10.1126/science.1131475

[10] C. Caizer, *Handbook of Nanoparticles* (eds. M. Aliofkhazraei) (Springer International Publishing, Cham, 2016), p. 475. doi: https://doi.org/10.1007/978-3-319-15338-4_24

[11] J. Park, K. An, Y. Hwang, J. G. Park, H. J. Noh, J. Y. Kim, J. H. Park, N. M. Hwang, and T. Hyeon, *Nat. Mater.*, **3**, 891 (2004). doi: https://doi.org/10.1038/nmat1251

[12] N. R. Jana, Y. Chen, and X. Peng, *Chem. Mater.*, **16**, 3931 (2004). doi: https://doi.org/10.1021/cm049221k

[13] A. B. Salunkhe, V. M. Khot, J. M. Ruso, and S. I. Patil, *RSC Adv.*, **5**, 18420 (2015). doi: https://doi.org/10.1039/C5RA00049A

[14] O. M. Lemine, K. Omri, B. Zhang, L. El Mir, M. Sajieddine, A. Alyamani, and M. Bououdina, *Superlattices Microstruct.*, **52**, 793 (2012). doi: https://doi.org/10.1016/j.spmi.2012.07.009

[15] J. Liu, L. Wang, J. Wang, and L. Zhang, *Mater. Res. Bull.*, **48**, 416 (2013). doi: https://doi.org/10.1016/j.materresbull.2012.10.060

[16] S. Guo, D. Li, L. Zhang, J. Li, and E. Wang, *Biomaterials*, **30**, 1881 (2009). doi: https://doi.org/10.1016/j.biomaterials.2008.12.042

[17] R. Tognato, A. R. Armiento, V. Bonfrate, R. Levato, J. Malda, M. Alini, D. Eglin, G. Giancane, and T. Serra, *Adv. Funct. Mater.*, **29**, 1804647 (2019). doi: https://doi.org/10.1002/adfm.201804647

[18] H. Ullah, Z. Haneef, A. Ahmad, I. S. Butler, R. N. Dara, and Z. Rehman, *Inorg. Chem. Commun.*, **153**, 110775 (2023). doi: https://doi.org/10.1016/j.inoche.2023.110775

[19] L. P. Zhu, H. M. Xiao, W. D. Zhang, G. Yang, and S. Y. Fu, *Cryst. Growth Des.*, **8**, 957 (2008). doi: https://doi.org/10.1021/cg700861a

[20] F. Fiévet, S. Ammar-Merah, R. Brayner, F. Chau, M. Giraud, F. Mammeri, J. Peron, J. Y. Piquemal, L. Sicard, and G. Viau, *Chem. Soc. Rev.*, **47**, 5187 (2018). doi: https://doi.org/10.1039/C7CS00777A

[21] Z. Xu, C. Shen, Y. Hou, H. Gao, and S. Sun, *Chem. Mater.*, **21**, 1778 (2009). doi: https://doi.org/10.1021/cm802978z

[22] L. Zhuang, W. Zhang, Y. Zhao, H. Shen, H. Lin, and J. Liang, *Sci. Rep.*, **5**, 9320 (2015). doi: https://doi.org/10.1038/srep09320

[23] N. Qin, W. Lin, J. Chen, D. Gao, Y. Liu, Y. Zhang, and Q. Yang,

New J. Chem., **48**, 9429 (2024).
doi: https://doi.org/10.1039/D4NJ01395F

[24] I.O.P. De Berti, M. V. Cagnoli, G. Pecchi, J. L. Alessandrini, S. J. Stewart, J. F. Bengoa, and S. G. Marchetti, *Nanotechnology*, **24**, 175601 (2013).
doi: https://doi.org/10.1088/0957-4484/24/17/175601

[25] N.L.N. Broge, F. Søndergaard-Pedersen, M. Roelsgaard, X. Hassing-Hansen, and B. B. Iversen, *Nanoscale*, **12**, 8511 (2020).
doi: https://doi.org/10.1039/D0NR01240H

[26] G. Villaverde-Cantizano, M. Laurenti, J. Rubio-Retama, and R. Contreras-Cáceres, *Reducing Agents in Colloidal Nanoparticle Synthesis* (eds. S. Mourdikoudis) (The Royal Society of Chemistry, 2021).
doi: https://doi.org/10.1039/9781839163623-00001